Influence of Pluronic® P123 Addition in the Synthesis of Bulk Ni Promoted MoS2 Catalyst. Application to the Selective Hydrodesulfurization of Sulfur Model Molecules Representative of FCC Gasoline

Valentin Hetier, Diego Peña, Alexandre Carvalho, Laurence Courthéoux, Valérie Flaud, Etienne Girard, Denis Uzio, Sylvette Brunet, Patrick Lacroix-Desmazes, Annie Pradel

catalysts

MDPI

Article

Influence of Pluronic® P123 Addition in the Synthesis of Bulk Ni Promoted MoS_2 Catalyst. Application to the Selective Hydrodesulfurization of Sulfur Model Molecules Representative of FCC Gasoline

Valentin Hetier [1], Diego Pena [2], Alexandre Carvalho [2], Laurence Courthéoux [1,*], Valérie Flaud [1], Etienne Girard [3], Denis Uzio [3], Sylvette Brunet [2,*], Patrick Lacroix-Desmazes [1] and Annie Pradel [1]

1 Institut Charles Gerhardt Montpellier (ICGM), Université de Montpellier, CNRS, ENSCM, 34090 Montpellier, France; valentin.hetier@enscm.fr (V.H.); valerie.flaud@umontpellier.fr (V.F.); patrick.lacroix-desmazes@enscm.fr (P.L.-D.); annie.pradel@umontpellier.fr (A.P.)

2 Institut de Chimie des Milieux et Matériaux de Poitiers (IC2MP), Université de Poitiers, UMR 7285 CNRS, 4 rue Michel Brunet, TSA 71106, 86073 Poitiers, France; diego.pena@univ-poitiers.fr (D.P.); alexandre.carvalho@univ-poitiers.fr (A.C.)

3 IFP Energies nouvelles, rond-point de l'échangeur de Solaize—BP 3 69360 Solaize, France; etienne.girard@ifpen.fr (E.G.); denis.uzio@ifpen.fr (D.U.)

* Correspondence: laurence.courtheoux@umontpellier.fr (L.C.); sylvette.brunet@univ-poitiers.fr (S.B.)

Received: 25 July 2019; Accepted: 18 September 2019; Published: 23 September 2019

Abstract: A way to improve hydrotreatment processes is to enhance the intrinsic activity of Ni or Co promoted MoS_2 catalysts that are commonly used in such reactions. The aim of this work was to investigate the impact of the presence of Pluronic® P123 as a structuring agent during the synthesis of Ni promoted MoS_2 catalysts (named NiMoS) in water at room temperature. A series of analyses, i.e., X-ray diffraction (XRD), chemical analysis, inductively coupled plasma mass spectrometry (ICP-MS), nitrogen adsorption-desorption isotherms, transmission electron microscopy (TEM) and X-ray photoelectron spectroscopy (XPS), helped in characterizing the NiMoS-P123 and NiMoS catalysts, the latter being prepared in the absence of polymer. Both compounds contained MoS_2 phase (~85 atomic% considering Mo atoms), a similar amount of mixed Ni-Mo-S phase (40–50% considering Ni) and some amount of NiS and Ni-oxidized impurity phases. The main differences between the two catalysts were a much larger specific surface area (126 $m^2 \cdot g^{-1}$ instead of 31 $m^2 \cdot g^{-1}$) and a better dispersion of the active phase as shown by the lower slab stacking (2.7 instead of 4.8) for NiMoS-P123, and the presence of C in NiMoS-P123 (9.4 wt.% instead of 0.6 wt.%), indicating an incomplete decomposition of the polymer during thermal treatment. Thanks to its larger specific surface area and lower slab stacking and therefore modification of active Mo site properties, the compound prepared in the presence of Pluronic® P123 exhibits a strong increase of the catalytic activity expressed per Mo atom for the transformation of 3-methylthiophene. Such improvement in catalytic activity was not observed for the transformation of benzothiophene likely due to poisonous residual carbon which results from the presence of Pluronic® P123 during the synthesis.

Keywords: NiMoS; Pluronic® P123; catalyst; hydrodesulfurization; 3-methylthiophene; benzothiophene

1. Introduction

Worldwide growth of the global mobility of people and merchandises, along with industrial activity, have resulted in a severe increase in airborne pollutants concentration in the last decades.

To counterbalance this, the production of cleaner fuels used for on-road and off-road transportations has been imposed to refiners. In particular, the reduction of sulfur content in gasoline and diesel cuts through hydrodesulfurization (HDS) processes have become essential to meet worldwide regulations [1,2]. This has consequently stimulated research and innovations in hydrotreatment processes and heterogeneous catalysts.

Conventional hydrotreating catalysts are based on Group 6 transition metal sulfides (MoS_2) usually promoted by Group 9 and 10 transition metals such as nickel or cobalt [3]. They are traditionally prepared by incipient wetness impregnation of supports such as alumina [3], zeolites [4], or graphitic carbons [5], by an aqueous solution of metal precursors and then activation by a sulfidation step. However, this preparation method often leads to a poor dispersion of the metal and limited metal loadings in contradiction with requirements for higher activity in hydrodesulfurization reactions. In order to improve the intrinsic activities of supported sulfide active phases, strategies based on a better control of the physicochemical properties—such as the morphology, size, and stacking of the MoS_2 slabs, electronic properties, or surface composition have been extensively described in literature [6].

A different approach for the development of highly active catalysts comes with the preparation of bulk hydrotreating Ni or Co promoted MoS_2 catalysts (named NiMoS or CoMoS) in order to maximize their activity per volume of reactor. This synthesis usually proceeds in two steps, i.e., the synthesis of mixed NiMo oxide phases by co-precipitation followed by a sulfidation step [7–10]. Alternatively, the direct synthesis of sulfide phases with thio precursors (i.e., without the sulfidation step of metal oxide intermediates) has been also described in the literature [11–13]. Noteworthy, in both cases, the obtained catalysts suffer from low specific surface areas. In order to get larger specific surface areas, the structuration of bulk MoS_2 catalysts with organic compounds such as surfactants, polymers, or ionic liquids can be considered [6]. For instance, several studies used polymers such as poly(vinyl pyrrolidone) (PVP) or poly(ethylene glycol) (PEG), which led to a decrease of the MoS_2 stacking [14,15] and to an increase of the specific surface area [16]. Under hydrothermal conditions, the MoS_2 synthesis templated by surfactants or polymers may also lead to different morphologies such as nano or microspheres, nanoflowers, or hexagonal particles [17–20]. Interestingly, the addition of organic compounds during the synthesis of Ni (or Co)-promoted MoS_2 catalysts has been less studied. Some papers report the synthesis, usually in hydrothermal conditions, of molybdenum oxide phases promoted by Ni, in the presence of polymers such as PVP [21,22] or PEG [23] but a further sulfidation step was required. In these studies, the presence of nickel sulfide phases has been observed in addition to the mixed Ni-Mo-S phase. Furthermore, although the oxide materials could present a specific surface area up to 144 $m^2 \cdot g^{-1}$, the sulfide catalysts displayed much lower surface areas, from 8 to 20 $m^2 \cdot g^{-1}$. Actually, the direct synthesis of the sulfide phase from sulfur precursors in the presence of organic structuring agents has been scarcely reported. Genuit et al. [24] reported the preparation of efficient bulk Co(Ni)MoS catalysts obtained with nonionic surfactants (poly(ethylene oxide) oligomers with aryl-alkyl tail), in a mixed water/ethylene glycol solution, leading to a specific surface area of 122 $m^2 \cdot g^{-1}$. For the hydrothermal synthesis of Ni-promoted MoS_2 in the presence of decalin, Yoosuk et al. [25] have shown that by increasing the temperature to 375 °C and the pressure up to 2.8 MPa, a very high specific surface area up to 250 $m^2 \cdot g^{-1}$ could be obtained. Recently, we have reported a first series of data on the preparation of Ni-promoted MoS_2 catalysts in the presence of an ionic liquid and their physicochemical characterization has shown different morphologies and an increase of the specific surface area depending on the amount of ionic liquid [26].

The present paper focuses on the consequences of the presence of a polymeric surfactant on the catalytic activity of a bulk NiMoS catalyst prepared by "soft chemistry" route in water. To do so, a commercial and cheap polymer, Pluronic® P123, was used to act as a steric stabilizer. This amphiphilic water-soluble poly(ethylene oxide)-*b*-poly(propylene oxide)-*b*-poly(ethylene oxide) triblock copolymer ($HO(CH_2CH_2O)_{20}(CH_2CH(CH_3)O)_{70}(CH_2CH_2O)_{20}H$), able to self-assemble in aqueous media, will interact with the water-insoluble MoS_x formed during the reaction. Physicochemical characterizations

based on nitrogen adsorption–desorption isotherms, X-ray diffraction, X-ray photoelectron spectroscopy, and transmission electron microscopy were carried out. Finally, the catalytic performances of bulk NiMoS were investigated for the transformation of two sulfur model molecules—3-methylthiophene and benzothiophene—representative of Fluid Catalytic Cracking (FCC) gasoline.

2. Results and Discussion

2.1. Catalysts Characterizations

The synthesis described in this paper is a very easy and very fast reaction performed in water at ambient temperature and pressure. The reaction directly leads to the sulfide catalysts. Indeed, the reaction between nickel nitrate and ammonium thiomolybdate is instantaneous and leads to a colloidal unstable black suspension according to the following suggested reaction [24]: $(NH_4)_2MoS_4$ + $Ni(NO_3)_2.6H_20 \rightarrow NiMoS_4 + 2NH_4NO_3 + 6H_2O$. The presence of Pluronic® P123 above its critical micellar concentration does not alter the kinetic of the reaction and a sterically stabilized black suspension is obtained as soon as the two precursor solutions are mixed.

Chemical analyzes of the materials before and after thermal treatment at 320 °C (under a reductive atmosphere of argon and 5% H_2) have been performed and are reported in Table 1. The amount of sulfur after thermal treatment varies from 35 wt.% for NiMoS to 31 wt.% for NiMoS-P123. The amount of nickel determined by inductively coupled plasma mass spectrometry (ICP) is higher for NiMoS (17.6 wt.%) than for NiMoS-P123 (12.9 wt.%). However, the Ni/Mo ratio is similar (≈0.5). As expected, only traces of C or H residue are visible in the absence of polymer. In contrast, when Pluronic® P123 is added, the carbon and hydrogen content are equal to 26.9 and 5.1 wt.%, respectively, before the thermal treatment. This corresponds to a H/C weight ratio of 0.19 very close to the theoretical value of the Pluronic® P123 (theoretical H/C weight ratio of 0.17). After thermal treatment at 320 °C, the carbon and hydrogen contents decrease to 9.4 and 1.1 wt.%, respectively, giving a H/C weight ratio of 0.11, which indicates that the organic residue does not correspond to Pluronic® P123 anymore. The remaining of a carbonaceous phase can be explained by an incomplete decomposition of the polymer trapped within the materials, during the heat treatment in a reductive H_2(5%)/Ar atmosphere. In an attempt to remove all carbonaceous residue, heat treatment at 500 °C has been performed. The elemental analysis showed similar result with 9.5 wt.% of C. It must be noticed that all the synthesis of NiMoS in the presence of organic compounds (solvent, surfactant, or polymer) described in the literature also reported the presence of similar amounts of carbon after thermal treatment [17,27–29].

Table 1. Impact of the presence of P123 on bulk NiMoS characteristics (specific surface area, elemental analysis (wt.%)) before and after thermal treatment at 320 °C.

Sample	S_{BET} (m^2.g)	C*	H*	S*	Ni**	Mo**	Ni/Mo**
NiMoS [a]		0.6	0.1	34.8			
NiMoS [b]	31	0.6	0.1	34.6	17.6	34.6	0.5
NiMoS-P123 [a]		26.9	5.1	21.5			
NiMoS-P123 [b]	126	9.4	1.1	30.9	12.9	27.6	0.5

* Determined by elemental analysis, ** Determined by inductively coupled plasma mass spectrometry ICP-MS, (**a**) before thermal treatment at 320 °C, (**b**) after thermal treatment at 320 °C.

The nitrogen adsorption–desorption curves of the NiMoS and NiMoS-P123 materials obtained after thermal treatment at 320 °C are represented in Figure 1. The isotherm featured for the NiMoS catalyst prepared without polymer is the signature of inter-particle capillary condensation (type II according IUPAC classification). On the other hand, the isotherm obtained for the NiMoS-P123 catalyst prepared with Pluronic® P123 corresponds to type IV isotherm characteristic of mesoporous materials [30]. Furthermore, the hysteresis loop can be attributed either to pore-blocking/percolation in a narrow range of pore necks or to cavitation-induced evaporation [31]. The pore size distribution of

the NiMoS-P123 catalyst (Figure 2) obtained by the BJH method from the desorption branch shows a narrow peak centered at 3.8 nm with a pore volume of 0.16 $cm^3 \cdot g^{-1}$. Considering the t-plot from Harkins and Jura law, it is possible to assert that no microporosity is evidenced in NiMoS-P123 catalysts but very few microporosities corresponding to 4 $m^2 \cdot g^{-1}$ should not be excluded in NiMoS. The specific surface areas of the catalysts have been determined by the BET method and are reported in Table 1. The addition of Pluronic® P123 generated specific surface area of 126 $m^2 \cdot g^{-1}$, four times higher than the surface of the NiMoS catalyst prepared without polymer (31 $m^2 \cdot g^{-1}$). Several authors have reported the large increase of the specific surface area of MoS_2 by using polymer such as polyvinyl pyrrolidone (92 $m^2 \cdot g^{-1}$) [16] or organic compound such as propylene carbonate (between 140 and 190 $m^2 \cdot g^{-1}$) [17]. Most of the studies on the synthesis of Ni-promoted MoS_2 catalysts concern the synthesis of oxides which are further sulfided just before the catalytic evaluations. In those cases, the specific surface area of the oxide phases could be increased by the use of PVP up to 144 $m^2 \cdot g^{-1}$ as reported by Liu [22]. But very small specific surface areas were obtained for the final NiMoS catalysts: less than 20 $m^2 \cdot g^{-1}$. To our knowledge, Genuit et al. [24] are the only ones who reported a specific surface area of 122 $m^2 \cdot g^{-1}$ for NiMoS catalyst prepared in one step and at ambient pressure without further sulfidation. This NiMoS catalyst has been obtained in the presence of Tergitol® surfactant in a mixture of water and ethylene glycol. The mechanism responsible of the increase of the surface area is not clearly detailed in the literature but the role of the organic phase seems to be the steric stabilization of the nuclei to prevent the particle growth. In this study, the addition of an amphiphilic polymer not only leads to a higher specific surface area but also to the formation of a mesoporosity. This may be due to an increase of the disorder of the MoS_2 slabs by the polymer. Furthermore, the remaining carbonaceous species due to an incomplete removal of the polymer during the washing and the thermal treatment steps may contribute to the formation of a mesoporous composite MoS_2-C phase.

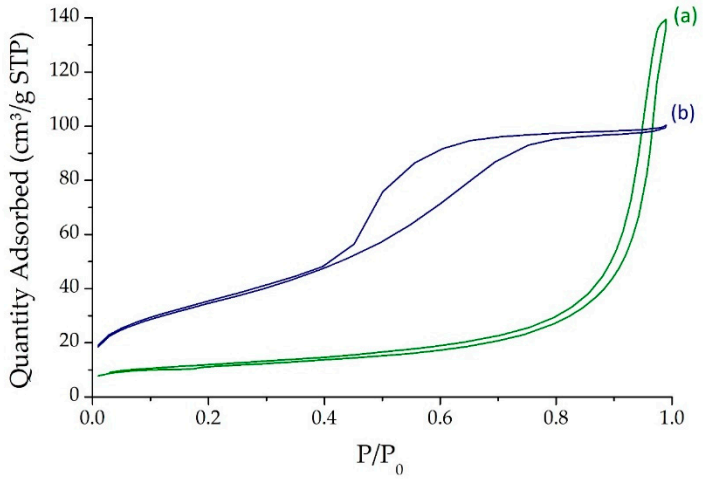

Figure 1. Nitrogen adsorption–desorption analysis for NiMoS prepared (a) without Pluronic® P123 and (b) with Pluronic® P123, and treated at 320 °C under H_2/Argon.

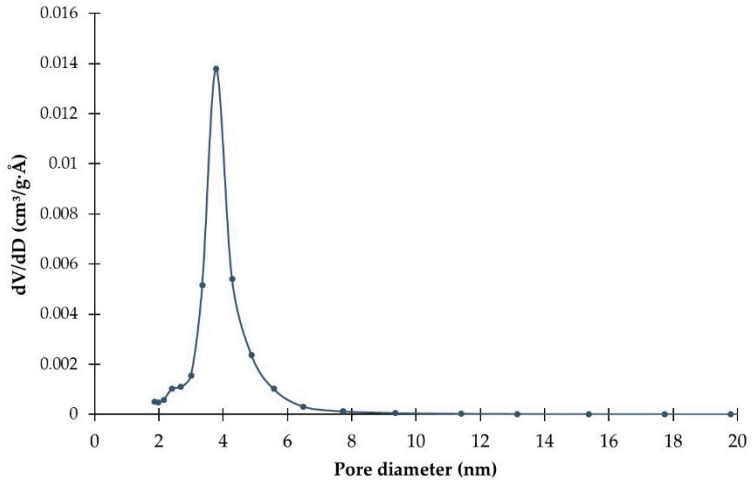

Figure 2. Pore size distribution for the NiMoS-P123 catalyst prepared with Pluronic® P123 and treated at 320 °C under H_2/Argon (from desorption branch of isotherm).

X-ray diffraction analyses have been performed on the NiMoS materials obtained after thermal treatment at 320 °C and the spectra are reported in Figure 3. The catalysts exhibited broad diffraction peaks, indicating a very poorly crystallized MoS_2 structure, particularly when the polymer is added (NiMoS-P123). Without polymer, a second phase corresponding to nickel sulfide NiS is also observed. The formation of nickel sulfide phase has already been observed in several synthesis of NiMoS catalysts [21,26,32]. This may be due to the reaction between the sulfur expelled during the thermal treatment and some Ni that is not used to form the mixed Ni-Mo-S phase. Yoosuk [25] claimed that the presence of a small amount of secondary phases Ni_3S_2 and NiS, for atomic ratio of Ni/(Ni+Mo) lower than 0.5, had no apparent detrimental effect on the conversion of dibenzothiophene (DBT) and 4,6-dimethyldibenzothiophene (4,6-DMDBT). This has been confirmed by Liu [21].

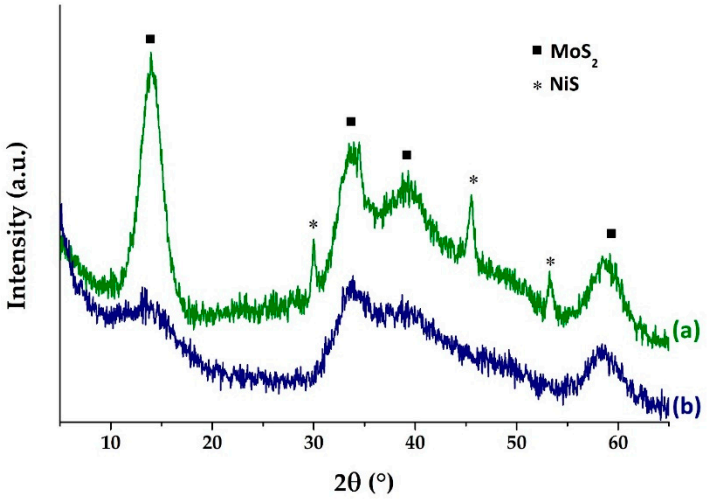

Figure 3. X-ray diffractograms of catalysts prepared (a) without Pluronic® P123 and (b) with Pluronic® P123, and thermally treated at 320 °C.

It is also very interesting to notice that the presence of an organic phase such as a polymer in our case, or a surfactant in the case of Xu, [28] led to a decrease or to the absence of the X-ray diffraction peaks attributed to the nickel sulfide phase. The disorder due to the organic phase may thus increase the amount of the Ni-Mo-S phase and/or lead to Ni_xS_y nano-crystallites that are too small to be characterized by X-ray diffraction method. To address this question and gain further insights in their chemical composition, the synthesized materials were analyzed by X-ray photoelectron spectroscopy

(XPS). According to the chemical analysis presented in Table 1 and to the Mo 3d, Ni 2p, and S 2p XPS spectra decomposition shown in Figures 4–7, the co-existence of MoS_2, NiMoS, NiS, and Ni_{ox} phases was confirmed. Indeed, the various MoS_2 (Mo $3d_{5/2}$ BE = 229.3 eV; S $2p_{3/2}$ BE = 162.2 eV), NiS (Ni $2p_{3/2}$ BE = 853.2 eV), Ni_{ox} (Ni $2p_{3/2}$ BE = 856.1 eV), and mixed phase Ni-Mo-S (Ni $2p_{3/2}$ BE = 854.3 eV) species were well identified. Quantitative analysis of XPS data helped in evaluating the S/Mo and Ni/(Ni+Mo) atomic ratios as well as the sulfidation rate of molybdenum (proportion of MoS_2 (%)) and the amount of Ni-Mo-S mixed phase (Table 2). The MoS_2 phase (S/Mo ratio between 2.3 and 2.5) was indeed formed in a large amount (around 85%), similar for the two catalysts. The Ni/(Ni+Mo) atomic ratios values ranging between 0.3 and 0.4 are closed to the one of the conventional $NiMo/Al_2O_3$ catalyst used in hydrotreatment processes. The mixed NiMoS phase was formed in a large amount (around 40–50 %). On the whole, the synthesis method proposed in this work led to an amount of Ni-Mo-S mixed phase in the material similar to the one observed for conventional supported catalyst (45%) [13]. While no oxidation of sulfur and subsequent formation of sulfates were noticed in the XPS spectra, the relative amount of Ni oxidized impurity phases, Ni_{ox} (41%) in the NiMoS-P123 sample was significantly higher than that of the reference NiMoS sample (17%). The increase of the Ni_{ox} phase for NiMoS-P123 may be explained by the release of oxygen due to the degradation of the polymer during the thermal treatment at 320 °C. In the case of NiMoS-P123, this increase in the Ni_{ox} phase was essentially counterbalanced by a decrease in the proportion of the Ni_xS_y phases. This also confirmed the works of Xu and al. [28] suggesting the formation of small Ni_xS_y crystals non detectable by X-ray diffraction.

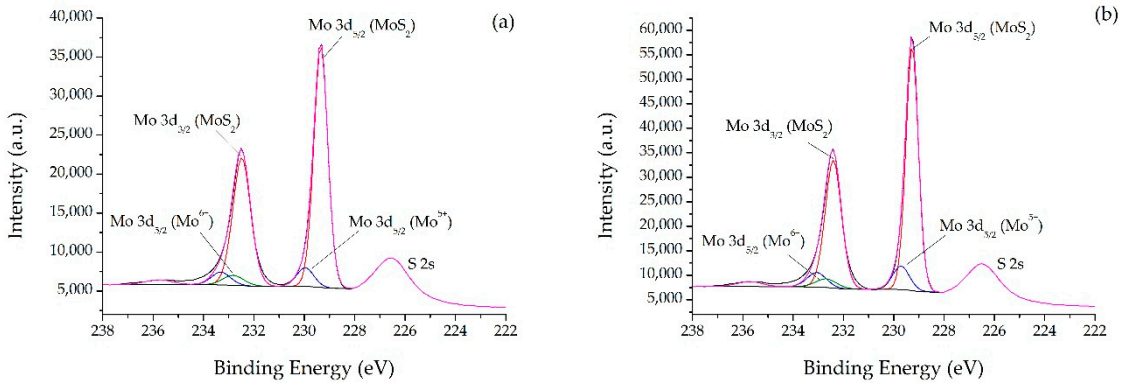

Figure 4. Mo 3d XPS spectra of NiMoS catalysts prepared (**a**) without Pluronic® P123 and (**b**) with Pluronic® P123, and treated at 320 °C.

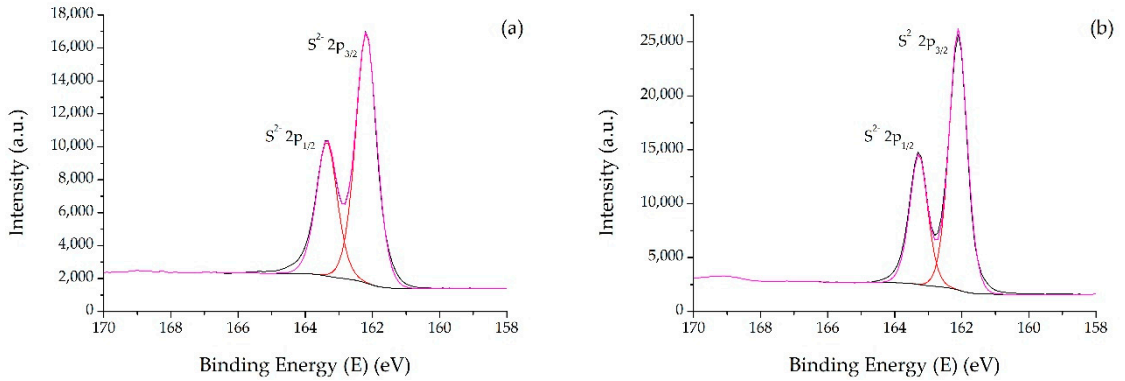

Figure 5. S 2p XPS spectra of NiMoS catalysts prepared (**a**) without Pluronic® P123 and (**b**) with Pluronic® P123, and treated at 320 °C.

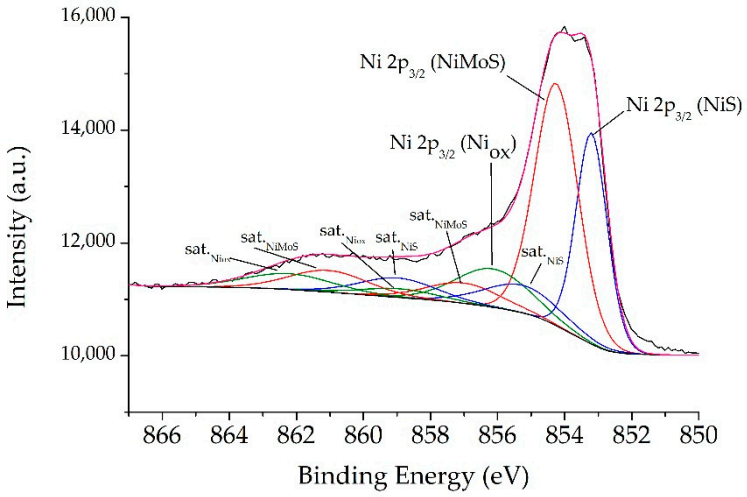

Figure 6. Ni 2p XPS spectra of NiMoS. The satellites of each phase have been labelled as sat.$_{phase}$.

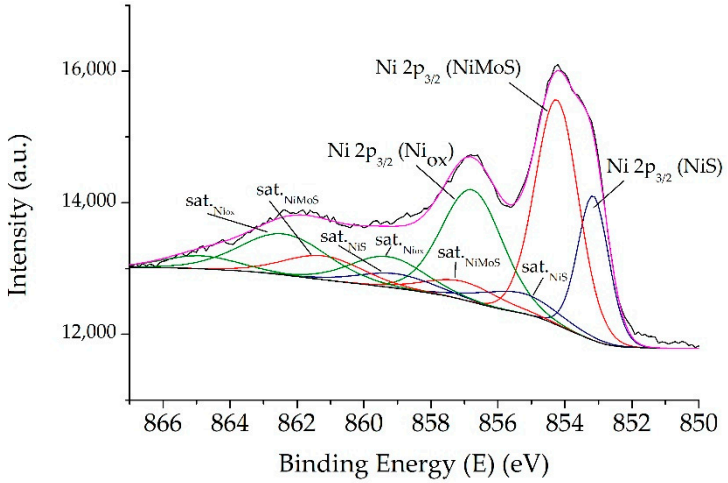

Figure 7. Ni 2p XPS spectra of NiMoS-P123. The satellites of each phase have been labelled as sat.$_{phase}$.

Table 2. Quantitative XPS analysis of the bulk catalysts after thermal treatment at 320 °C and sulfidation at 400 °C.

			Mo Fraction (rel.%)			Ni Fraction (rel.%)			
Catalyst	**S/Mo**	**Ni/(Ni+Mo)**	**Mo^{5+}**	**Mo^{6+}**	**MoS_2**	**NiMoS**	**NiS**	**Ni_{ox}**	**$(Ni/Mo)_{slab}$ ***
NiMoS	2.5	0.37	9	5	86	48	35	17	0.56
NiMoS-P123	2.3	0.28	11	5	84	38	21	41	0.45

* promoter ratio in the active phase slab determined using $(Ni/Mo)_{slab} = \frac{C_{NiMoS}}{C_{MoS_2}}$ where C_X is the absolute concentration of Ni(Mo) in the NiMoS(MoS_2) species (atomic%).

Notably, the peak corresponding to the MoS_2 (002) plan at $2\theta \approx 14°$ in the X-ray diffraction patterns of NiMoS samples decreased drastically with the addition of Pluronic® P123 (Figure 3). The height of the peak being linked to the number of stacked slabs, this decrease is attributed to a decrease in the stacking of the MoS_2 slabs for the NiMoS-P123 [33]. The size of the particles can be estimated using the Scherrer formula. Owing to the small peak in the case of NiMoS-P123, the particles diameter size has only been estimated for NiMoS and was found to be around 3 nm (Table 3). The position of the (002) peak, $2\theta \approx 14°$, corresponds to an interspace layer of 6.3 Å and thus to a stacking of 5–6. The decrease of the crystallinity of the MoS_2 phase and the low stacking due to the addition of polymer such as PEG or PVP have been depicted by several authors [14–16,18] and was said to be consistent with an

expansion of the interlayers by Wu [15]. However, in the present work, it is difficult to point the peak at 14° precisely and thus to attest to any displacement on the basis of X-ray diffraction patterns.

Table 3. MoS_2 particles size determined by XRD, stacking of the MoS_2 layers determined by XRD and TEM images, average length of the layers determined by TEM and average ratio edge-to-corner of MoS_2 slabs.

	XRD		TEM				
Catalyst	**S [a] (nm)**	**St [b]**	**St [b]**	**L [c] (nm)**	**Lmin (nm)**	**Lmax (nm)**	**$(f_e/f_c)_{Mo}$**
NiMoS	3	6	4.8	3.8	2.2	9.3	4.4
NiMoS-P123	-	-	2.7	3.3	1.1	10.2	3.7

[a] MoS_2 particle size (S), [b] average stacking (St), [c] average length (L), ratio edge-to-corner of a MoS_2 slab ($(f_e/f_c)_{Mo}$).

The interlayer of the NiMoS slabs was also measured using TEM images (Figure 8) and corresponds to 6.3 Å for NiMoS, which is consistent with the X-ray diffraction results and matches the (002) basal plane of crystalline MoS_2. Regarding the NiMoS-P123 catalyst, an interlayer of 6.6 Å was measured, which indicates a small expansion. The length and stacking of MoS_2 slabs were also estimated from TEM analysis (Figures 9 and 10, respectively) while the average length and stacking are reported in Table 3. As expected from the XRD analyses, the stacking is low and the average length of the layer is short: 3.8 nm for NiMoS and 3.3 nm for NiMoS-P123. The addition of Pluronic® P123 during the synthesis led to a decrease of the average stacking from 4.8 without polymer down to 2.7 layers in the presence of polymer. Furthermore, the distribution of the stacking differs between the two samples. Indeed, for NiMoS-P123, 77% of the observed MoS_2 particles have 2 or 3 layers and almost 10% have monolayer. But for NiMoS, the distribution is centered at 4–5 layers without any monolayers. In the literature, most works report a stacking higher than 5 for the syntheses of bulk catalysts carried out without any structuring agent and a decrease of the MoS_2 stacking or even no stacking for the syntheses with the addition of an organic compound; however, most of these studies dealt with the synthesis of MoS_2 and not NiMoS [15,29]. The ratio edge-to-corner of a MoS_2 slab ($(f_e/f_c)_{Mo}$) has been calculated (Table 3) from TEM images according to Nikulshin [34]. This ratio is slightly lower for NiMoS-P123 (3.7) than for NiMoS (4.4), in agreement with the decrease of the average slab length.

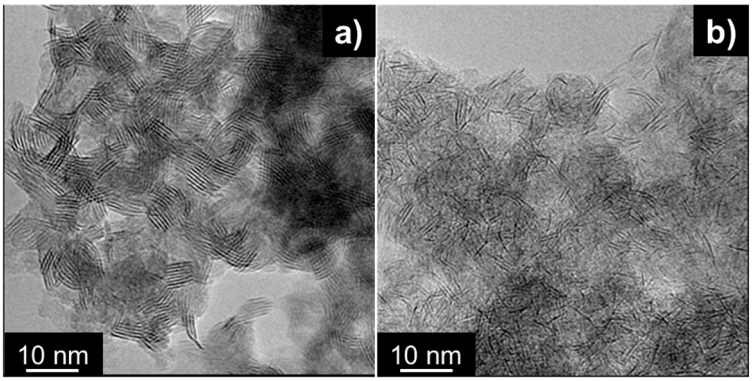

Figure 8. TEM images of NiMoS catalysts prepared (**a**) without Pluronic® P123 and (**b**) with Pluronic® P123, and treated at 320 °C.

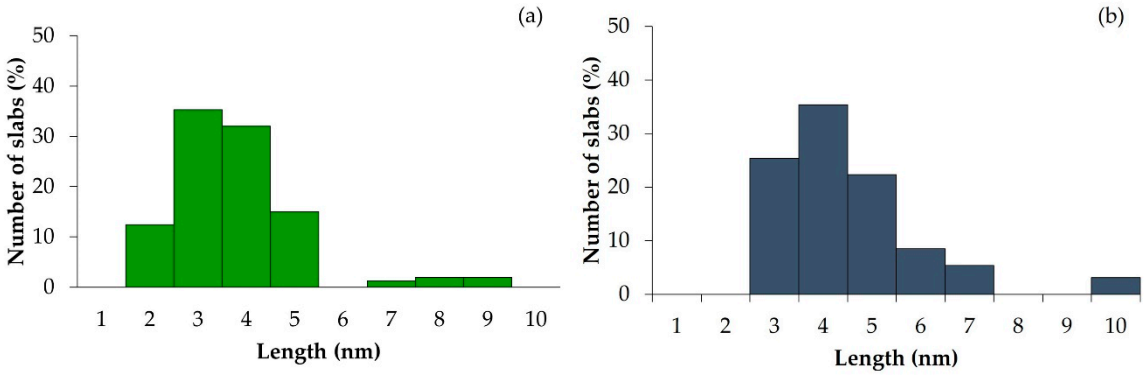

Figure 9. Distribution of the slab length for NiMoS catalysts prepared (**a**) without Pluronic® P123 and (**b**) with Pluronic® P123, and treated at 320 °C.

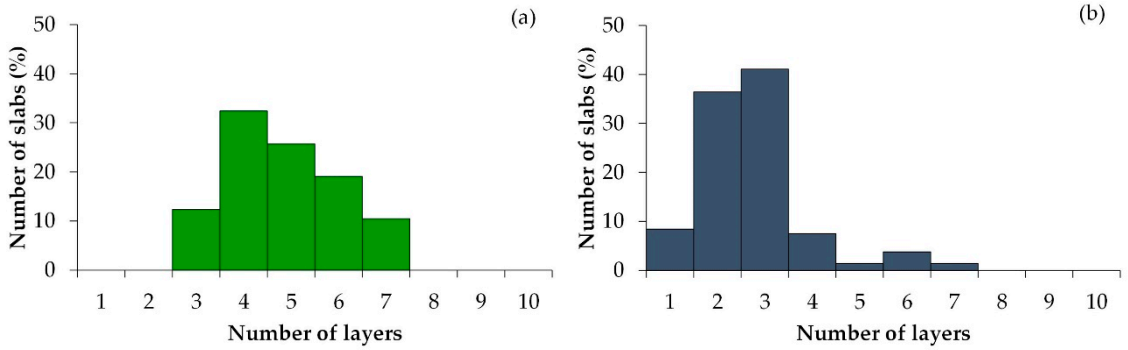

Figure 10. Distribution of the number of layers for NiMoS catalysts prepared (**a**) without Pluronic® P123 and (**b**) with Pluronic® P123, and treated at 320 °C.

2.2. *Catalytic Performances in the Transformation of Model Molecules Representative of FCC Gasoline*

Both NiMoS-P123 and NiMoS catalysts were evaluated in the hydrodesulfurization of 3-methylthiophene (3MT) and benzothiophene (BT).

Data related to the transformation of 3MT are shown in Figures 11 and 12, and in Tables 4 and 5. The NiMoS-P123 sample synthesized in the presence of P123 exhibited an increase of around 30% in the catalytic activity per gram for the transformation of 3MT although it corresponds to a decrease of activity when taking into account its specific surface area (Table 4). This indicated that the improvement was not the only consequence of the increase in specific surface area but also to a modification of the properties of the molybdenum active sites. As a matter of fact, the intrinsic activity (per Mo atom) is doubled when the polymer is present during the synthesis. For the two catalysts, the conversion increases with the contact time (Figure 11) and for a same contact time (0.25 s), the conversion is higher for NiMoS-P123. For the whole range of conversion, the product distribution is similar for both catalysts (Figure 12). The olefins are the main products with a majority of 2MB2N (2-methybut-2-ene) and small amounts of 2MB1N and 3MB1N. When the conversion increases, the amount of isopentane (i-C5)—the final hydrogenation product—increases and becomes the main product for conversion close to 100%. This mainly corresponds to a decrease in the formation of 2MB2N. These results are in agreement with the well-established reaction scheme where the HDS of 3MT involved consecutive reactions with olefins as intermediates [35]. No modification of selectivities is noticed between the two materials (Table 5).

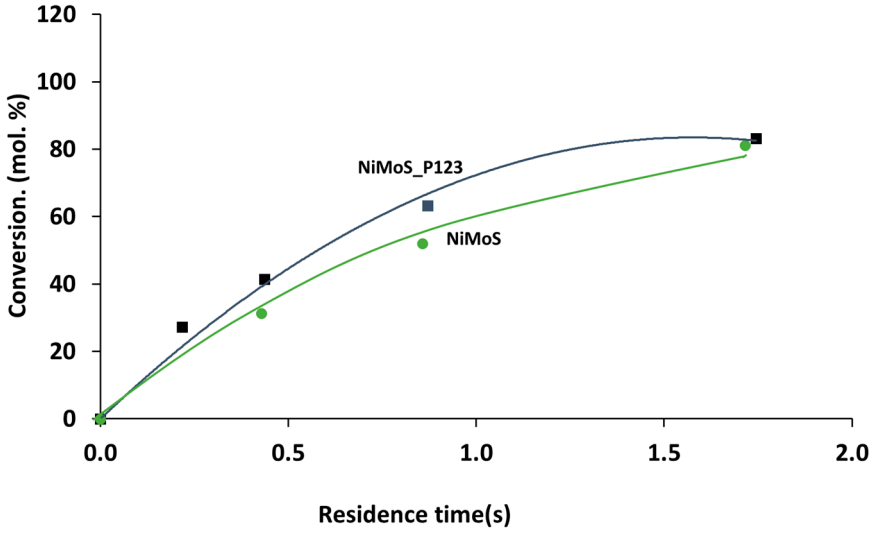

Figure 11. Transformation of 3MT. Conversion versus residence time over NiMoS-P123 (square) and NiMoS (circle) (T = 250 °C; P = 20 bar; H_2/HC = 360 NL/L).

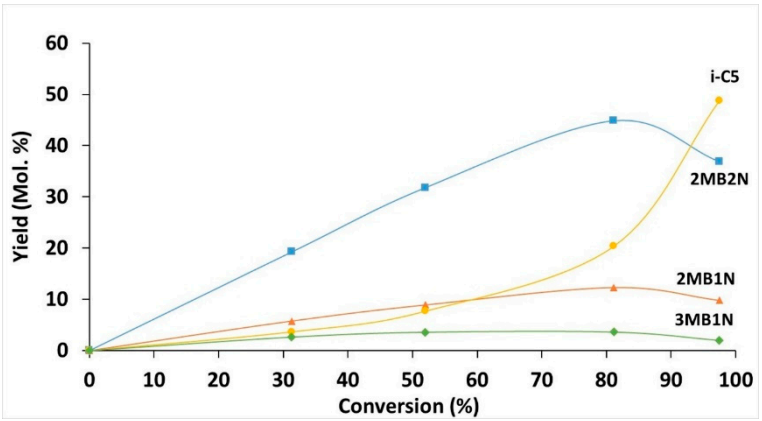

Figure 12. Transformation of 3MT. Product distribution versus conversion (T = 250 °C; P =20 bar; H_2/HC = 360 NL/L, NiMoS) (2MB2N: 2-methylbut-2-ene, 2MB1N: 2-methylbut-1-ene, 3MB1N: 3-methylbut-1-ene).

Table 4. Transformation of sulfur model compounds (3MT, BT). Activity per gram, per square meter and per Mo atom (T = 250 °C; P = 20 bar; H_2/HC = 360 NL/L, isoconversion: around 30%).

	3MT			BT		
	$mmol \cdot g_{cata}^{-1} \cdot h^{-1}$	10^{-2} mmol $\cdot m^2 \cdot h^{-1}$	10^{-21} $mmol \cdot at_{Mo}^{-1} \cdot h^{-1}$	$mmol \cdot g_{cata}^{-1} \cdot h^{-1}$	10^{-2} $mmol \cdot m^2 \cdot h^{-1}$	10^{-21} $mmol \cdot at_{Mo}^{-1} \cdot h^{-1}$
NiMoS	2.2	7.1	1.2	4.2	13.6	2.2
NiMoS-P123	3.1	2.5	2.2	3.7	2.9	2.6

Table 5. Transformation of 3MT. Comparison of selectivities (T = 250 °C; P = 20 bar; H_2/HC = 360 NL/L, isoconversion: around 30%) (2MB2N: 2-methylbut-2-ene, 2MB1N: 2-methylbut-1-ene, 3MB1N: 3-methylbut-1-ene, 3MTHT: 3-methyltetrahydrothiophene, i-C5/=C5 = isopentane/(2MB2N + 2MB1N + 3MB1N)).

Catalyst	iC5 %	3MB1N %	2MB1N %	2MB2N %	iC5/=C5 %
NiMoS	11.7	8.4	18.4	61.5	0.13
NiMoS-P123	13.2	5.7	18.2	62.9	0.15

Hydrodesulfurization (HDS): iC5 + 3MB1N + 2MB1N + 2MB2N.

Data related to the transformation of BT are shown in Figures 13 and 14, and in Tables 4 and 6. Conversely to data obtained for the transformation of 3MT, the NiMoS catalyst has higher activities per gram and per square meter than the sample prepared with P123 in the transformation of BT (Figure 13, Table 4). However, the activity per molybdenum atom remained similar. As shown in Figure 14 for NiMoS catalyst, two products are formed, according to the reaction scheme previously established [35]: dihydrobenzothiophene (DHBT) corresponding to the partial hydrogenation of BT and ethylbenzene (EB) as the HDS product, this one being the main product.

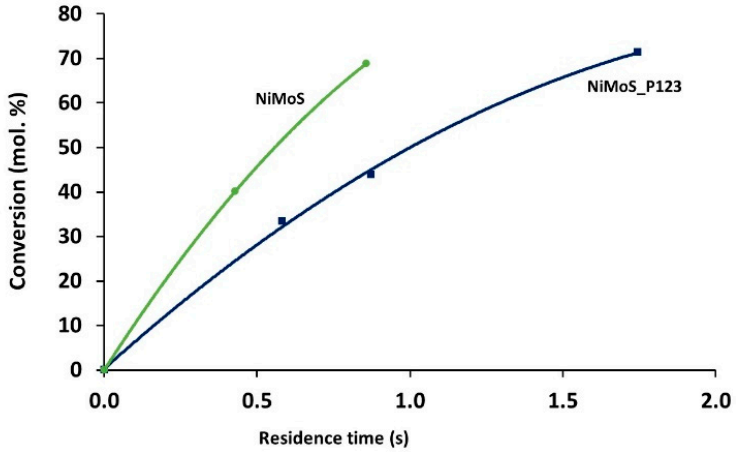

Figure 13. Transformation of BT. Conversion versus residence time over NiMoS (circle) and NiMoS-P123 (square) (T = 250 °C; P = 20 bar; H_2/HC = 360 NL/L).

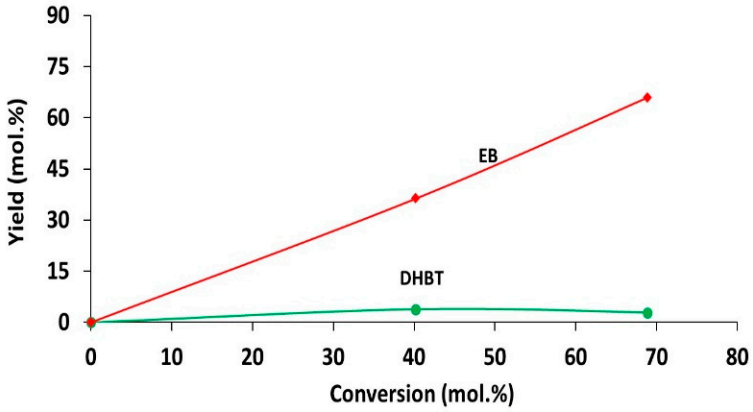

Figure 14. Transformation of BT. Product distribution versus conversion (T = 250 °C; P = 20 bar; H_2/HC = 360 NL/L, NiMoS)(EB: ethylbenzene, DHBT: dihydrobenzothiophene).

Table 6. Transformation of BT. Comparison of selectivities (T = 250 °C; P = 20 bar; H_2/HC = 360NL/L, isoconversion: around 30%) (DHBT: dihydrobenzothiophene, EB: ethylbenzene).

Catalyst	DHBT %	EB %
NiMoS	3.9	96.1
NiMoS-P123	6.8	93.2

When comparing the two catalysts (Table 4), it appears that BT is clearly more reactive than 3MT over the NiMoS catalyst, and has a similar reactivity to 3MT over NiMoS-P123 catalyst. The first result agrees with data reported in the literature and dealing with the reactivity of the two sulfur molecules in presence of $CoMoS/Al_2O_3$ [35]. It has been explained by a stronger adsorption of BT compared to that of 3MT. The second data is more surprising. Some differences in structure and/or morphology of the two catalysts due to the presence or not of polymer during the synthesis must be at the bottom of the understanding.

If taking into account the uncertainty on the data (20% for XPS), both chemical and XPS analysis show that the Ni/Mo ratio and quantity of active Ni-Mo-S phase are similar in the two catalysts (Tables 1 and 2). However, some differences between the two compounds are observed. Upon the addition of Pluronic® P123, the specific surface area of the compound increased from 31 to 126 $m^2 \cdot g^{-1}$, the average slab stacking decreased from 4.8 to 2.7 and finally, a large amount of C remained trapped in the compound prepared in presence of polymer, even after an heat treatment at 320 °C (9.4 wt.% for NiMoS-P123 compared to 0.6 wt.% for NiMoS) (Table 1). The two tested sulfur molecules differ in their adsorption properties and in the way their transformation preferentially proceeds.

Indeed, as reported previously for the transformation of 2MT [36], 3MT involves mainly C-S bond ruptures and can be adsorbed and reacts in all active sites located on the edges (sulfur and metallic) of MoS_2 slabs. The main way involved in BT transformation is the hydrogenation way to form dihydrobenzothiophene as an intermediate, followed by C–S bond breaking to produce ethylbenzene. In this case, a flat adsorption of BT could be involved on metallic edges or on rim sites in agreement with the rim-edge model [37]. It has already been reported in the literature that the presence of carbonaceous phase in a catalyst could decrease the accessibility of some active sites, especially the ones involved in the hydrogenation way [36,38,39]. Therefore, the presence of carbon due to an incomplete decomposition of Pluronic® P123 is particularly detrimental in the case of BT. It is a poison of the most favorable sites for its transformation and might also be at the origin of steric hindrance for these large molecules.

In the case of 3MT, the decrease in active hydrogenating sites might be counterbalanced by an increase in the number of accessible active sites due to the much larger specific surface area and decrease in average slab packing. Its smaller size compared to BT might also less suffer from steric hindrance due to carbon.

On the whole, the presence of P123 during the synthesis results in a markedly increase of the transformation of 3MT (a 30% increase for the activity per gram and a doubled intrinsic activity (per Mo atom)). Whereas, the catalytic activities per gram and per Mo atom for the transformation of BT change only by ±15%, whether the polymer was present or not during the synthesis. Such results are interesting in the perspective of an industrial use where FCC feed comprises several sulfur molecules. As a matter of fact, it was shown recently [35] in a model feed representative of an FCC feed, that the transformation of 3MT was inhibited by the presence of BT. In the case of NiMoS-P123, its improved activity for 3MT might therefore allow an easier sulfur removal when this catalyst is used. It should then be easier to reach the level of sulfur requested by regulations (10 ppm of sulfur).

3. Materials and Methods

3.1. Catalyst Preparation

The triblock copolymer Pluronic® P123 (EO_{20}-PO_{70}-EO_{20}; EO: ethylene oxide; PO: propylene oxide), nickel nitrate $Ni(NO_3)_2{\cdot}6H_2O$ (99.99%), ammonium tetrathiomolybdate $(NH_4)_2MoS_4$ (99.97 %), and ethanol were purchased from Sigma Aldrich (Sigma Aldrich, St. Louis, MO, USA). All products were used without further purification. H_2 (5%)/Ar (99.95%) was provided by Linde gas (Linde gas, Munich, Germany).

NiMoS catalysts were prepared as follows: $(NH_4)_2MoS_4$ (4 mmol) and $Ni(NO_3)_2{\cdot}6H_2O$ (4 mmol) were separately dissolved in 40 mL of pure H_2O or in 40 mL of an aqueous solution of Pluronic®P123 (0.2 mmol). The two solutions were then mixed with gentle magnetic stirring for 30 s, at room temperature and under an air atmosphere. The reaction mixture was then stored for 12 h at room temperature and the particles were separated by centrifugation (40,000 rpm, 4 h) using a Beckman Coulter Optima XPN ultracentrifuge with a 45 TI rotor and 70 mL PC tubes. Three washings with 80 mL of water were performed (centrifugation at 40,000 rpm, 4 h), followed by a final washing step with 80 mL of ethanol. The particles were finally recovered by centrifugation (20,000 rpm, 4 h) in 94 mL PP tubes. All the products were then dried under primary vacuum for 12 h at T = 25 °C. Finally, the powder was heated under an atmosphere of 5% hydrogen in argon from room temperature to 320 °C at 5 °C.min^{-1}, held 2 h at 320 °C, and cooled down to room temperature at the same rate under argon. This temperature has been chosen as a compromise: At a lower temperature, the decomposition of Pluronic® P123 would decrease (potentially increasing the carbon residue), whereas at a higher temperature, the number of MoS_2 layers would increase. The catalysts were then stored under vacuum before use.

3.2. NiMoS Characterizations

The specific surface areas were determined by nitrogen adsorption–desorption using a Micromeritics tristar apparatus after a night of degassing at 120 °C (Micromeritics, Norcross, GA, USA). Elemental analysis (sulfur, hydrogen, nitrogen, and carbon amounts) was carried out using an Elementar Vario Micro Cube (Elementar, Langenselbold, Germany) while the molybdenum and nickel amounts were measured by inductively coupled plasma mass spectrometer (ICP-MS) using a SPECTRO ARCOS ICP-AOS analyzer (SPECTRO Analytical Instruments, Kleve, Germany). X-ray powder diffraction (XRD) patterns were recorded with a Malvern Panalytical X'pert PRO X-ray diffractometer by using Cu radiation (λ = 1.5406 Å) (Malvern Panalytical, Royston, U.K.). A JEOL JEM2100F (JEOL, Tokyo, Japan) transmission electron microscope (TEM) was used to characterize the MoS_2 phase (length and stacking).

XPS spectra were recorded using a KRATOS AXIS ultra spectrometer (Kratos Analytical, Manchester, U.K.) equipped with a (150 W) Al Kα monochromatic source (hν = 1486.6 eV). Before analysis, catalysts were sulfided at 400 °C during 10 h by a mixing of H_2S (10 molar %)/H_2 at atmospheric pressure and stored in Schlenk under argon to avoid oxidation resulting in the formation of sulfates at the surface. They were identified with reference samples drawn from the handbook of X-ray photoelectron spectroscopy [40], NIST X-ray Photoelectron Spectroscopy Database (NIST Standard Reference Database 20, Web Version 3.4, Gaithersburg, MD, USA). The calibration has been made with the carbon peak of contamination at 284.6 eV. For each catalyst, the metal and sulfur peaks were identified according to their binding energies [41,42]. The elemental surface composition of the catalysts, and therefore, the sulfur/metal atomic ratio (S/Me) and the active phase formation were determined from the area of the metal and sulfur peaks (the uncertainty of the value is around 20%).

3.3. Catalytic Performances

As previously reported [35], catalytic activity measurements were carried out in a fixed bed reactor at 523 K under a total pressure of 2 MPa with a ratio H_2/feed of 360 NL/L. First, the catalyst was

sulfided in situ under H_2S/H_2 flow (10 mol% H_2S) for 10 h at 673 K at atmospheric pressure. These operating conditions correspond to those of the industrial process [36].

Catalytic performances of the NiMoS bulk catalysts were measured for the transformation of a single component feed including a sulfur model molecule alone (corresponding to 1000 ppm S) (0.3 wt.% of 3MT or 0.42 wt.% of BT) in n-heptane. The sulfur model feeds were injected in the reactor by a HPLC Gilson pump (307 series, pump's head: 5 cm^3). 3-methylthiophene (98% purity), benzothiophene (95% purity), and n-heptane (>99% purity) were purchased from Sigma-Aldrich (Sigma Aldrich, St. Louis, MO, USA). They were used without further purification. Hydrogen sulfide (10 mol% in mixture with H_2) and hydrogen was purchased from Air Liquide (Air Liquide, Paris, France).

The different partial pressures of the reactants, H_2S and H_2 introduced are reported in Table 7. n-heptane was not converted under these experimental conditions. No catalyst deactivation was observed for all the experiments.

Table 7. Partial pressures (kPa) of the different compounds for the sulfidation step and the transformation of the different feeds.

Pressure (kPa)	Sulfidation	3MT	BT
P_{H2S}	10	0	0
P_{3MT}	0	200	0
P_{BT}	0	0	200
P_{H2}	90	1360	1360
P_{nC7}	0	637	637
P_{TOT}	100	2000	2000

The reaction products were injected on-line by means of an automatic sampling valve into a Varian gas chromatograph equipped with a PONA capillary column and a flame ionization detector as in previous works [35]. Desulfurized products, resulting from the transformation of 3-methylthiophene and benzothiophene are designated as HDS products. Regarding the transformation of the 3-methylthiophene, HDS products (mainly pentanes and pentenes) are the main observed products according to the reaction scheme described in the literature [36] (Scheme 1).

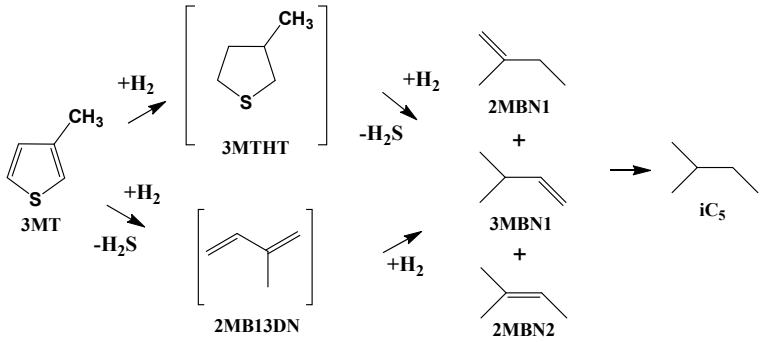

Scheme 1. Transformation of 3-methythiophene (3MT). 3-methyltetrahydrothiophene (3MTHT), 2-methyl-but-1-ene (2MBN1), 2-methyl-but-2-ene (2MBN2), 3MBN1 (3-methyl-but-1-ene), isopentane (iC5).

The transformation of BT led mainly to ethylbenzene as HDS product and also to tetrahydrobenzothiophene (THBT) corresponding to the partially hydrogenation of BT (Scheme 2).

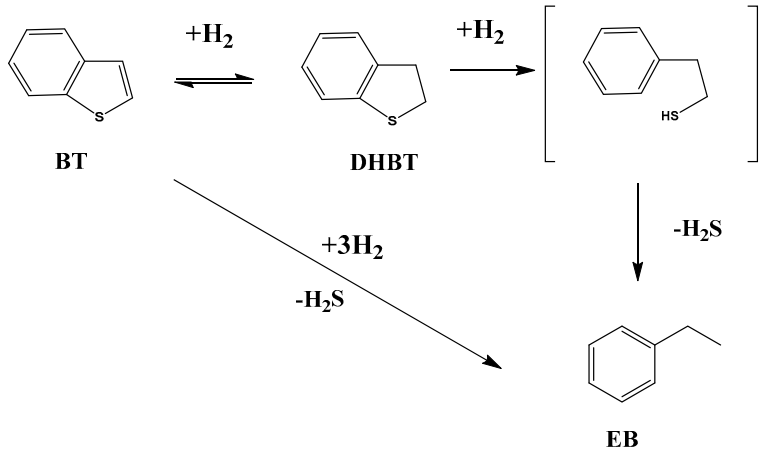

Scheme 2. Transformation of benzothiophene (BT): dihydrobenzothiophene (DHBT), ethylbenzene (EB).

The contact time is defined as the ratio between the total amount of feed and the mass of catalyst. 3MT and BT reactivities are defined as the number of moles of products formed per hour and per gram of catalyst and were calculated at conversion lower than 30% in a differential regime.

4. Conclusions

The influence of addition of polymer Pluronic® P123 during the synthesis of bulk NiMoS catalyst on the structure, morphology, and catalytic properties has been investigated. It has been shown that, while no change in the Ni/Mo ratio and amount of Ni-Mo-S active phase could be observed, the compound prepared in the presence of polymer has a much larger specific surface area, a lower average slab stacking, and a higher amount of C than the catalyst prepared in the absence of polymer.

These differences affected the catalytic properties of the two tested sulfur molecules, 3MT, and BT, in different ways. The presence of carbon in NiMoS-P123 was detrimental to the catalytic activity for BT transformation, probably due to some steric effect and the poisoning of active sites favorable to hydrogenation, the main transformation way for BT. In the case of 3MT which can be adsorbed on all active sites, the negative effect of residual carbon due to an incomplete decomposition of Pluronic® P123 is probably counterbalanced by an increase in the number of accessible active sites due to the large specific surface area and low average slab stacking in NiMoS-P123. As a result, the catalytic activity, either per gram or Mo atoms of NiMoS-P123 is higher for the 3MT transformation than the activity of NiMoS.

Author Contributions: Conceptualization: D.U., S.B., P.L.-D., L.C.; formal analysis: V.H., V.F., D.P., A.C., E.G.; investigation, V.H., D.P., A.C.; writing—original draft preparation: L.C.; writing—review and editing, A.P., D.U., S.B., P.L.-D.; supervision: A.P., L.C., S.B., P.L.-D.; project administration: S.B.; funding acquisition: A.P., D.U., S.B.

Funding: This work was funded by the French ANR, Programme National de Recherche N° ANR-16-CE07-0029-01—ASSCATA, a joint project between the Centre National de la Recherche Scientifique (CNRS), the universities of Montpellier and Poitiers and IFPEN Lyon.

Acknowledgments: The authors thank Dominique Foix from IPREM, Université de Pau et des pays de l'Adour, Pau (F) for valuable discussions on XPS data.

Conflicts of Interest: The authors declare no conflict of interest.

References

1. Directive 2009/30/CE L140/88. Available online: https://eur-lex.europa.eu/legal-content/FR/TXT/HTML/?uri=CELEX:32009L0030 (accessed on 21 July 2019).
2. Available online: TransportPolicy.nethttps://www.transportpolicy.net/?s=sulfur (accessed on 23 April 2019).
3. Chapuis, T.; Hudebine, D.; Souchon, V. *Catalysis by Transition Metal Sulfides: From Molecular Theory to Industrial Application*; Technip Edition: Paris, France, 2013; pp. 547–578.

4. Sun, Y.; Wang, H.; Prins, R. Hydrodesulfurization with classic Co–MoS_2 and Ni–MoS_2/-Al_2O_3 and new Pt–Pd on mesoporous zeolite catalysts. *Catal. Today* **2010**, *150*, 213–217. [CrossRef]
5. Pinilla, J.L.; Purón, H.; Torres, D.; de Llobet, S.; Moliner, R.; Suelves, I.; Millan, M. Carbon nanofibres coated with Ni decorated MoS2 nanosheets as catalyst for vacuum residue hydroprocessing. *Appl. Catal. B* **2014**, *148–149*, 357–365. [CrossRef]
6. Wang, S.; An, C.; Yuan, J. Synthetic Fabrication of Nanoscale MoS_2-Based Transition Metal Sulfides. *Materials* **2010**, *3*, 401–433. [CrossRef]
7. Alvarez, L.; Espino, J.; Ornelas, C.; Rico, J.L.; Cortez, M.T.; Berhault, G.; Alonso, G. Comparative study of MoS_2 and Co/MoS_2 catalysts prepared by ex situ/insitu activation of ammonium and tetraalkylammonium thiomolybdates. *J. Mol. Catal. A Chem.* **2004**, *210*, 105–117. [CrossRef]
8. Liu, H.; Yin, C.; Li, B.L.X.; Li, Y.; Chai, Y.; Liu, C. Effect of Calcination Temperature of Unsupported NiMo Catalysts on the Hydrodesulfurization of Dibenzothiophene. *Energy Fuels* **2014**, *28*, 2429–2436. [CrossRef]
9. Liu, H.; Liu, C.; Yin, C.; Chai, Y.; Li, Y.; Liu, D.; Li, B.L.X.; Wang, Y.; Li, X. Preparation of highly active unsupported nickel–zinc–molybdenumcatalysts for the hydrodesulfurization of dibenzothiophene. *Appl. Catal. B* **2015**, *174–175*, 264–276. [CrossRef]
10. Song, W.; Lai, W.; Chen, Z.; Cao, J.; Wang, H.; Lian, Y.; Yang, W.; Jiang, X. Fabrication of 3D Porous Hierarchical NiMoS Flowerlike Architectures for Hydrodesulfurization Applications. *ACS Appl. Nano Mater.* **2018**, *1*, 442–454. [CrossRef]
11. Fuentes, S.; Diaz, G.; Pedraza, F.; Rojas, H.; Rosas, N. The influence of a new preparation method on the catalytic properties of CoMo and NiMo sulfides. *J. Catal.* **1988**, *113*, 535–539. [CrossRef]
12. Lai, W.; Chen, Z.; Zhu, J.; Yang, L.; Zheng, J.; Yi, X.; Fang, W. A NiMoS flower-like structure with self-assembled nanosheets as high-performance hydrodesulfurization catalysts. *Nanoscale* **2016**, *8*, 3823–3833. [CrossRef]
13. Lamic, A.F.; Daudin, A.; Brunet, S.; Legens, C.; Bouchy, C.; Devers, E. Effect of H_2S partial pressure on the transformation of a model FCC gasoline olefin over unsupported molybdenum sulfide-based catalysts. *Appl. Catal. A* **2008**, *344*, 198–204. [CrossRef]
14. Liang, S.; Zhou, J.; Liu, J.; Pan, A.; Tan, Y.; Chen, T.; Fang, G. PVP-assisted synthesis of MoS_2 nanosheets with improved lithium storage properties. *CrystEngComm* **2013**, *15*, 4998–5002. [CrossRef]
15. Wu, Z.; Wang, D.; Sun, A. Surfactant-assisted fabrication of MoS_2 nanospheres. *J. Mater. Sci.* **2010**, *45*, 182–187. [CrossRef]
16. Gu, P.; Zhao, C.; Wen, T.; Ai, Y.; Zhang, S.; Chen, W.; Wang, J.; Hu, B.; Wang, X. Highly U(VI) immobilization on polyvinyl pyrrolidine intercalated molybdenum disulfide: Experimental and computational studies. *Chem. Eng. J.* **2019**, *35*, 1563–1575. [CrossRef]
17. Afanasiev, P. Synthesis of finely divided molybdenum sulfide nanoparticles in propylene carbonate solution. *J. Solid State Chem.* **2014**, *213*, 158–164. [CrossRef]
18. Tang, G.; Wang, Y.; Chen, W.; Tang, H.; Li, C. Hydrothermal synthesis and characterization of novel flowerlike MoS_2 hollow microspheres. *Mater. Lett.* **2013**, *100*, 15–18. [CrossRef]
19. Tang, G.; Sun, J.; Wei, C.; Wu, K.; Ji, X.; Liu, S.; Tang, H.; Li, C. Synthesis and characterization of flowerlike MoS_2 nanostructures through CTAB-assisted hydrothermal process. *Mater. Lett.* **2012**, *86*, 9–12. [CrossRef]
20. Wu, Z.; Wang, D.; Sun, A. Surfactant-assisted preparation of hexagonal molybdenum disulfide nanoparticles. *Mater. Lett.* **2009**, *63*, 2591–2593. [CrossRef]
21. Liu, H.; Liu, Q.; Zhang, J.; Yin, C.; Zhao, Y.; Yin, S.; Liu, C.; Suna, W. PVP-assisted synthesis of unsupported NiMo catalysts with enhanced hydrodesulfurization activity. *Fuel Process. Technol.* **2017**, *160*, 93–101. [CrossRef]
22. Liu, H.; Yin, C.; Li, X.; Chai, Y.; Li, Y.; Liu, C. Effect of NiMo phases on the hydrodesulfurization activities of dibenzothiophene. *Catal. Today* **2017**, *282*, 222–229. [CrossRef]
23. Yin, C.; Zhao, L.; Bai, Z.; Liu, H.; Liu, Y.; Liu, C. A novel porous ammonium nickel molybdate as the catalyst precursor towards deep hydrodesulfurization of gas oil. *Fuel* **2013**, *107*, 873–878. [CrossRef]
24. Genuit, D.; Afanasiev, P.; Vrinat, M. Solution syntheses of unsupported Co(Ni)–Mo–S hydrotreating catalysts. *J. Catal.* **2005**, *235*, 302–317. [CrossRef]
25. Yoosuk, B.; Song, C.; Kim, J.H.; Ngamcharussrivichai, C.; Prasassarakich, P. Effects of preparation conditions in hydrothermal synthesis of highly active unsupported NiMo sulfide catalysts for simultaneous hydrodesulfurization of dibenzothiophene and 4,6-dimethyldibenzothiophene. *Catal. Today* **2010**, *149*, 52–61. [CrossRef]

26. Leyral, G.; Ribes, M.; Courthéoux, L.; Uzio, D.; Pradel, A. Synthesis and Structuring of Ni MoS_2 by using an Ionic Liquid. *Eur. J. Inorg. Chem.* **2012**, 4967–4971. [CrossRef]
27. Xiong, Y.; Xie, Y.; Li, Z.; Li, X.; Zhang, R. Micelle-assisted fabrication of necklace-shaped assembly of inorganic fullerene-like molybdenum disulfide nanospheres. *Chem. Phys. Lett.* **2003**, *382*, 180–185. [CrossRef]
28. Xu, J.; Huang, T.; Fan, Y. Highly efficient NiMo/SiO_2-Al_2O_3 hydrodesulfurizatio ncatalyst prepared from gemini surfactant-dispersed Mo precursor. *Appl. Catal. B* **2017**, *203*, 839–850. [CrossRef]
29. Afanasiev, P.; Xia, G.F.; Berhault, G.; Jouguet, B.; Lacroix, M. Surfactant-Assisted Synthesis of Highly Dispersed Molybdenum Sulfide. *Chem. Mater.* **1999**, *11*, 3216–3219. [CrossRef]
30. Rouquerol, F.; Rouquerol, J.; Sing, K.S.W.; Llewellyn, P.; Maurin, G. *Adsorption by Powders and Porous Solids*; Academic Press: Cambridge, MA, USA, 2014.
31. Thommes, M.; Kaneko, K.; Neimark, A.V.; Olivier, J.P.; Rodriguez-Reinoso, F.; Rouquerol, J.; Sing, K.S.W. Physisorption of gases, with special reference to the evaluation of surface area and pore size distribution (IUPAC Technical Report). *Pure Appl. Chem.* **2015**, *87*, 1051–1069. [CrossRef]
32. Leyral, G.; Brillouet, S.; Rousseau, J.; Richard, F.; Mamede, A.S.; Courtheoux, L.; Pradel, A.; Ribes, M.; Brunet, S. Effect of the presence of ionic liquid during the NiMoS bulk preparation in the transformation of decanoic acid. *Appl. Catal. A* **2017**, *532*, 120–132. [CrossRef]
33. Joensen, P.; Frindt, R.F.; Morrison, S.R. Single-layer MoS_2. *Mater. Res. Bull.* **1986**, *21*, 457–461. [CrossRef]
34. Nikulshin, P.A.; Ishutenko, D.I.; Mozhaev, A.A.; Maslakov, K.I.I.; Pimerzin, A.A. Effects of composition and morphology of active phase of CoMo/Al_2O_3 catalysts prepared using Co_2Mo_{10}–heteropolyacid and chelating agents on their catalytic properties in HDS and HYD reactions. *J. Catal.* **2014**, *312*, 152–169. [CrossRef]
35. Santos, A.S.d.; Girard, E.; Leflaive, P.; Brunet, S. Competitive adsorptions between thiophenic compounds over a CoMoS/Al_2O_3 catalyst under deep HDS of FCC gasoline. *Appl. Catal. A* **2019**, *570*, 292–298. [CrossRef]
36. Brunet, S.; Mey, D.; Pérot, G.; Bouchy, C.; Diehl, F. On the hydrodesulfurization of FCC gasoline: A review. *Appl. Catal. A* **2005**, *278*, 143–172. [CrossRef]
37. Daage, M.; Chianelli, R.R. Structure-function relation in molybdenum sulfide catalysts: The "rim-edge" model. *J. Catal.* **1994**, *149*, 414–427. [CrossRef]
38. Sadakane, O. Desulfurization method for catalytically cracked gasoline. Eur. Pat. EP0745660A1, 4 December 1996.
39. Hatanaka, S. Hydrodesulfurization of Selective Catalytic Cracked Gasoline. *Catal. Surv. Asia* **2005**, *9*, 87–93. [CrossRef]
40. Moulder, J.F. *Handbook of X-ray Photoelectron Spectroscopy*; Perkin-Elmer Cordporation: Waltham, MA, USA, 1992.
41. Guichard, B.; Roy-Auberger, M.; Devers, E.; Legens, C.; Raybaud, P. Aging of Co(Ni)MoP/Al_2O_3 catalysts in working state. *Catal. Today* **2008**, *130*, 97–108. [CrossRef]
42. Ninh, T.K.T.; Massin, L.; Laurenti, D.; Vrinat, M. A new approach in the evaluation of the support effect for NiMo hydrodesulfurization catalysts. *Appl. Catal. A* **2011**, *407*, 29–39. [CrossRef]